National University of Ireland Galway

Final year project

Calculating the Magnetic Field Around a Neutron Star

Jack Collins, 13388696

supervised by
Prof. Andrew Shearer

March, 2017

Abstract

In this project, the magnetic field around a neutron star was modelled using the equations of Muslimov and Harding [Muslimov and Harding, 2005]. An interactive 3D visualisation of the magnetic field lines surrounding the star was created. The changing of polar cap shape as magnetic inclination angle varies was investigated and found to agree with previous publications. Observed emissions for stars with different properties were plotted and the change in these emissions as particular properties of the star are varied was studied. The pulse profile for the Crab pulsar was modelled using estimates for magnetic inclination angle and viewing angle from previous publications. This was compared to observations and found to be in agreement.

Contents

Abstract **i**

1 Introduction **1**
1.1 Project Aims . . . 1
1.2 What are Neutron Stars? . . . 1
1.3 Discovery of Pulsars/Neutron Stars . . . 1
1.4 Current Research at NUI Galway . . . 2

2 Neutron Star Magnetosphere **3**
2.1 Magnetic Field Geometry . . . 3
2.2 The Deutsch Model . . . 4
2.2.1 Background . . . 4
2.2.2 Model Summary . . . 4
2.3 Muslimov and Harding Model . . . 5
2.3.1 Magnetic Coordinates . . . 5
2.3.2 Model Description . . . 5

3 Modelling Neutron Star Emission **6**
3.1 Polar Cap Model . . . 7
3.2 Outer Gap Model . . . 7
3.3 Synchrotron Radiation . . . 7
3.4 Properties Affecting Emissions . . . 8

4 Design of Program **8**
4.1 Classes . . . 9
4.1.1 'Star' class . . . 9
4.1.2 'Fieldline' class . . . 9
4.2 Algorithms . . . 10
4.2.1 Calculation of Field Lines . . . 10
4.2.2 Determining Observer's View of Emissions . . . 10
4.2.3 Storing and Retrieving Emissions Results . . . 11
4.3 Optimisations . . . 11

5 Results **12**
5.1 Visualisation . . . 12
5.2 Polar Cap Shape . . . 12
5.3 Emissions Calculations . . . 14
5.3.1 Plotting Emissions . . . 14
5.3.2 Varying Magnetic Inclination Angle, χ . . . 15
5.3.3 Varying Emission Distance, R_{LC} . . . 15
5.4 Comparison to Observed Emissions: Crab Pulsar . . . 17

6 Discussion **19**
6.1 Difficulties . . . 19
6.2 Sources of Error . . . 19

6.3 Future improvements 20

7 Conclusion **21**

Appendix **22**

Muslimov and Harding Equations 22

Downloading and running the program 23

Bibliography **24**

1 Introduction

1.1 Project Aims

The aim of this project was to model the magnetic field around a neutron star, and to create visualisations to aid in developing an intuition for and allowing insight into the behaviour of these objects. This project was part of ongoing research at the National University of Ireland, Galway (NUIG) and as such it was desired that any tools, techniques and results from this project would contribute to the overarching objective of locating the region of the neutron star magnetic field where emissions originate, and the mechanism by which this occurs.

1.2 What are Neutron Stars?

Neutron stars are extremely compact stars approximately twice the mass of the sun with a radius of only about 10 kilometres. They are formed from the supernovae of stars with about 10-30 times the mass of the sun. Neutron stars rapidly rotate, with the fastest known rotating with a frequency of 716 Hz [Hessels et al., 2006]. They have extremely strong magnetic fields between 10^8 and 10^{15} Gauss (Earth's varies between 0.25 and 0.65 Gauss) and extremely strong surface gravity, about one-tenth that of a black hole. Neutron stars demonstrate extreme physics. They operate at the limits of current theories and in many cases beyond the limits.

1.3 Discovery of Pulsars/Neutron Stars

The idea of neutron stars and their origin in supernovae explosions was first proposed in 1933 by Baade and Zwicky in a talk at the meeting of the American Physical Society.[1] This followed the discovery of the neutron by Chadwick in 1932. The existence of white dwarves as stars in which electron degeneracy pressure had been overcome had already been theorised, and the discovery of the neutron permitted the assumption that stars in which neutron degeneracy pressure was overcome could also exit. It was thought that such small, dense objects would be extremely dim and would only be observed indirectly, eg. on collision with another star.

In 1967, Jocelyn Bell Burnell, a graduate student at the University of Cambridge, first discovered a rapidly repeating signal in the reading of the x-ray telescope with which she was conducting a project. This signal was a very steady series of pulses with a period of 1.377 seconds [Shapiro and Teukolsky, 2008]. After eliminating the possibility of errors from artificial sources, it became clear that this signal was from a natural source. This source was called a pulsar.

By 1968, three important facts had been established about pulsars:

1. They had high frequency, with periods between 0.033 s and 3 s.
2. They were extremely accurate clocks, with the rate of change of period being very small.
3. This small change in period would only increase period, never decrease it.

[1] Russian physicist Lev Landau wrote a paper in 1931 which suggested the possibility of neutron stars, but the neutron had not yet been discovered and his reasoning violated quantum mechanics. [Yakovlev et al., 2013, Landau, 1938]

Object	Mass (M)	Radius (R)	Mean Density (g cm^{-3})	Surface Potential (GM/Rc^2)
Sun	$M_\odot$	$R_\odot$	1	10^{-6}
White Dwarf	$\lesssim M_\odot$	$\sim 10^{-2} R_\odot$	$\lesssim 10^7$	$\sim 10^{-4}$
Neutron Star	$\sim 1 - 3 M_\odot$	$\sim 10^{-5} R_\odot$	$\lesssim 10^{15}$	$\sim 10^{-1}$
Black Hole	Arbitrary	$2GM/c^2$	$\sim M/R^3$	~ 1

$M_\odot = 1.989x10^{33} g, R_\odot = 6.9599x10^{10} cm$

Table 1: Comparison of Compact Objects [Shapiro and Teukolsky, 2008]

From this information important deductions could be made about the nature of the objects creating this pulsed emission. In 1968, Gold published a paper [Gold, 1968] which argued that the observed radio pulsars must be rapidly rotating neutron stars. He showed that neutron stars could account for the incredibly stable pulse period. He predicted that a small increase in period would occur as the pulsar slowly lost rotational energy. This was before observations of the Crab pulsar slowing down were made. Further, in 1969 he showed the implied energy loss of a neutron star was roughly the same as the energy required to power the Crab nebula [Shapiro and Teukolsky, 2008].

1.4 Current Research at NUI Galway

Due to their extremely strong magnetic fields, rapid rotation, high temperature, and high energy emission, neutron stars are ideal objects for pushing physical theories to their limits. The combination of all these extreme aspects means that it is necessary to apply many simplifying assumptions when attempting to model their behaviour. In fact 40 years after their discovery, there is no agreement on what physical processes cause the emissions we observe, or even where these emissions originate relative to the star [de Burca, 2016]. The region of origin of emissions is one of the biggest unsolved problems in our understanding of neutron stars.

At NUI Galway, an attempt to answer some of these questions about neutron stars has been made using an 'inverse mapping' approach. This approach involves modelling the intensity and polarisation of the emissions of a pulsar, as observed by a distant observer. All of the unknown parameters are cycled through. The results of all these calculations are compared to actual observations made from Earth of real pulsars, and the best fitting result then gives an indication of how and where the emission is occurring. This work is known as the Pulsar Optical Reverse Engineering Code (POREC).

The inverse mapping approach works as follows:

1. create synchrotron radiation for each point in a volume above the magnetic pole of the star.
2. compute the set of light curves (polarisation) for each observer angle $0° - 180°$
3. statistically choose the best fit to observed data
4. locate region of origin of best fitting emissions

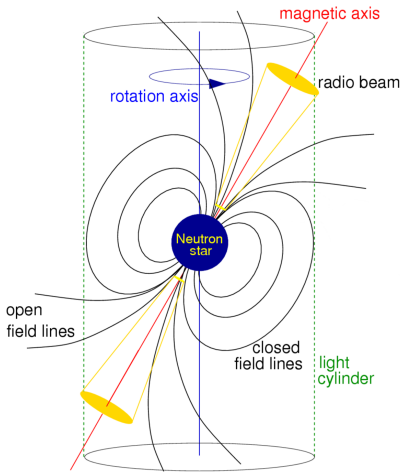

Figure 1: Neutron Star Magnetic Field Geometry. Note the magnetic axis is inclined to the axis of rotation, and the presence of open and closed field lines. [Lorimer and Kramer, 2005]

2 Neutron Star Magnetosphere

2.1 Magnetic Field Geometry

There are several important elements which make up the geometry of the magnetic field of the neutron star:

Magnetic Axis: A very important thing to note is that, in general, the magnetic axis and the rotation axis of the star are not aligned. The angle between them is known as the magnetic inclination angle or pulsar obliquity, and is denoted by χ. This has a profound effect on the geometry of the magnetic field. Due to the superconducting properties of neutron stars, it is assumed that the field is "frozen into" the star. This means that the magnetic axis rotates with star.

(Speed of) Light Cylinder: As the magnetic field gets further and further from the star, its velocity must increase in order to maintain corotation with the star. As the velocity of the field approaches the speed of light, this corotation can no longer hold and the field instead propagates into space as a spiral type structure [O'Connor, 2004]. This limit forms an imaginary cylinder around the star at which corotation break downs. The radius of the light cylinder can be calculated from the period of rotation of the star P, and the speed of light c.

$$R_{LC} = \frac{cP}{2\pi} \tag{1}$$

Magnetic Field Lines: There are two categories of magnetic field lines: open field lines and closed field lines. Closed field lines are field lines which remain within the star's light cylinder. These corotate with the star, and form closed loops. Open field lines are those which reach the light cylinder. This leads to the breaking down of their corotation, and spiralling off into space. Thus, open field lines do not return to the star. Charged particles only move along the open field lines, which means that these are the field lines from which we see emissions in the form of synchrotron

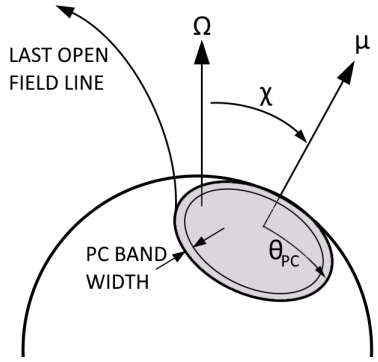

Figure 2: Neutron Star Polar Cap with axis of rotation Ω, magnetic axis μ, magnetic inclination angle χ.

radiation - as discussed in section 3.3.

Polar Cap: The polar cap is the region surrounding the magnetic pole of the star defined by the last open field lines. Any field line which has its initial position within the polar cap is an open field line and will hit the light cylinder. Any field line which starts outside the polar cap is a closed field line and will return to the star. For this project only the north polar cap was investigated, though there is also a polar cap at the south pole defined by where the last closed field lines from the north pole return to the star. The polar cap band indicated in Figure 2, is the area on the inner side of the polar cap boundary from which emitting field lines were created in simulations later in this project.

2.2 The Deutsch Model

2.2.1 Background

In 1953, H. W. Babcock had observed periodic variations of the magnetic field strength of certain stars [Babcock and Cowling, 1953]. These observations could be explained by either the "magnetic oscillator" or "oblique rotator" model. The magnetic oscillator theory relied on internal oscillations to explain the periodic reversal of a star's magnetic field. These were later shown to be unlikely to account for the periodic reversal of the magnetic field [Cowling, 1952]. So in his paper, Deutsch aimed to advance the oblique rotator model [Deutsch, 1955]. This theory explained the observations as due to the magnetic field of the star being symmetric about an axis at an angle to the axis of rotation and being carried with the star as it rotated.

2.2.2 Model Summary

The Deutsch model for the magnetic field is an analytic model based on standard dipole magnetic field. It is assumed that a star is a perfectly conducting, sharply bounded sphere in a vacuum.

Deutsch considers two inertial reference frames; one at rest with respect to the origin of the star, and one momentarily at rest with respect to a point of matter within the star. The internal magnetic and electric fields of the star are calculated in each frame. From Ohm's Law and the

infinite conductivity of the star assumption, the condition

$$\mathbf{E} = -\mu_0 \mathbf{V} \times \mathbf{H} \tag{2}$$

is derived. Here, E is the electric field vector, H represents the magnetic field and $\mathbf{V} = \omega \times \mathbf{r}$ is the local velocity of rotation measured from the first reference frame. The condition for the magnetic field to be "frozen into" the star

$$\mathbf{H}(r, \theta, \phi, t) = r_0 H_r(r, \theta, \lambda) + \theta_0 H_\theta(r, \theta, \lambda) + \phi_0 H_\phi(r, \theta, \lambda), \tag{3}$$

where λ is an azimuthal coordinate measured from a fixed meridian, is also noted. It is shown that these two conditions in combination satisfy Maxwell's equations admitting solutions which are symmetrical about a magnetic axis, at an angle to the axis of rotation.

Next, the external magnetic fields are found for a star in vacuum. This is done by considering a magnetic field with a particular form, symmetrical about a magnetic axis. This particular solution satisfies Maxwell's equations outside the star for charge density and electric current density being 0. The boundary conditions are enforced and the general solution for a field of the particular form found.

This field has the property that near the surface of the star the electric field vector has a component along the magnetic field vector which would accelerate charged particles to very high energies. Deutsch mentions that this is the least valid assumption made as it is improbable that near a real star the density can be low enough for such acceleration processes to occur as a star's corona leads to a more gradual decrease in conductivity. The assumption that the star is a sharply bounded sphere with infinite conductivity is much more valid. Both of these assumptions are perhaps more correct for a neutron star than for any other type of star.

2.3 Muslimov and Harding Model

2.3.1 Magnetic Coordinates

For this project the "magnetic" coordinate system used by Muslimov and Harding was adopted. This system uses polar coordinates with the polar axis parallel to the magnetic axis. In this system we have normalised radial coordinate $\eta = r/R$ (radial coordinate r, stellar radius R), polar angle θ measured from the magnetic axis, and azimuthal angle ϕ measured anti-clockwise from the meridian passing through the rotation axis. The magnetic inclination angle is denoted by χ.

2.3.2 Model Description

In their 2005 paper, Muslimov and Harding propose an analytical 3D model of the open field line region of a neutron star magnetosphere [Muslimov and Harding, 2005]. The fundamental differences to the Deutsch model are the assumptions that the electric charge density and the current density are not zero in the region surrounding the star, and that at higher altitude, where the effect of rotation becomes increasingly important, the electric field (in the inertial reference frame) is mostly determined by rotation. Another notable difference between the two approaches is that Deutsch's solution is presented in spherical coordinates with the polar axis along the rotation axis

whereas this solution uses magnetic coordinates - as discussed in section 2.3.1.

Muslimov and Harding begin by identifying the main physical effects distorting the geometry of the open-field line configuration within the light cylinder. These are decided to be

- magnetospheric rotation
- relativistic flow of charges along the open field lines
- $E \times B$-drift of out-flowing charges

These effects enter Maxwell's equations as first or second order terms in the radial distance. Separating the multiple terms allows a simplified version of Maxwell's equations to be solved for each effect to determine corrections to the static magnetic field that each causes. This method can be written as

$$\mathbf{B} = \mathbf{B}^d + \mathbf{B}^{(1)} + \mathbf{B}^{(2)} + \mathbf{B}^{(2*)} \tag{4}$$

where $\mathbf{B}^d$ is a pure magnetic dipole, $\mathbf{B}^{(1)}$ is the correction for the charge flow along open field lines, $\mathbf{B}^{(2)}$ is the distortion caused by rotation of the dipole, and $\mathbf{B}^{(2*)}$ is due to the $E \times B$-drift of the out-flowing charges.

The solution employs the space-charge-limited longitudinal current calculated in the electrodynamic model of Muslimov and Tsygan [Muslimov and Tsygan, 1992] and is valid up to very high altitudes approaching the light cylinder.

The resulting solutions (included in the appendix) show that at high altitudes the open magnetic field lines significantly deviate from those of a static dipole and tend to focus into a cylindrical bundle, swept back in the direction opposite to the rotation, and also bent towards the rotational equator.

3 Modelling Neutron Star Emission

The mechanism by which neutron stars convert their rotational energy into the observed pulsing emissions is poorly understood. None of the current competing theoretical models is satisfying. It is believed that the mechanism responsible for radio emissions is different to that responsible for higher energy emissions. This is because radio emissions of pulsars are known to be coherent process with coherent curvature radiation as the most promising mechanism [Becker et al., 2009]. For higher energy emissions however, a coherent radiation mechanism is not required. Optical pulsars are believed to have only one source of emission; incoherent synchrotron radiation. There is no agreement on the location of emissions in high-energy pulsars [Shapiro and Teukolsky, 2008]. There are two main types of emissions models: the polar cap model for which the emission region is very close to the the polar caps, and the outer gap model in which emissions stem from a region closer to the star's light cylinder.

The central problem with simulating pulsar emission is the large number of unconstrained variables. The magnetic inclination angle, and viewing angle is not known for certain for any pulsar. By varying even just these two parameters, it is possible to run simulations using different models

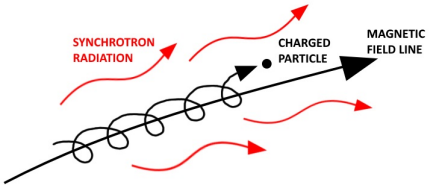

Figure 3: Forward directed synchrotron radiation from particle spiralling along magnetic field line.

and closely recreate the same observed emissions.

For the purposes of this project, emissions were modelled approximately as synchrotron radiation from the field lines. Beyond this, no particular emissions model was chosen as the variation of observed emissions with emission distance from the surface of the star was investigated.

3.1 Polar Cap Model

In the polar cap model, emission occurs within tens of kilometers of the polar cap. It is generally accepted radio emission occurs from within a few pulsar radii of the polar cap, with the frequency depending on the height of this location. The polar cap model is unsuccessful in accurately predicting high energy emission [de Burca, 2016].

3.2 Outer Gap Model

Outer gaps are regions above the null charge surface (where the corotation charge density changes sign) extending to the speed of light cylinder. Plasma lost from this gap cannot be replenished from the stellar surface, and a charge depleted region with significant $E \cdot B$ is developed. This is the location of the particle acceleration [Shapiro and Teukolsky, 2008].

The outer gap model places the emission region high up in the pulsar magnetosphere, approaching the light cylinder. In this model, high and low energy emissions occur in different locations. In 1986, Cheng, Ho and Ruderman [Cheng et al., 1986] argued that there were only three types of outer gap which could form and, of these, only the gap along the last open field lines was sustainable [de Burca, 2016].

3.3 Synchrotron Radiation

A charged particle which is accelerated emits radiation. Synchrotron radiation occurs when a charged particle is accelerated in a curved path ($\mathbf{a} \perp \mathbf{v}$) [Wiedemann, 2003]. When the particle has relativistic speeds, this radiation is directed in the direction of motion in a narrow cone.

In the case of neutron stars, the alignment of the strong electric and magnetic fields at the star's surface near the polar caps leads to the spiralling of charges along the magnetic field lines. As the velocity of these charges approaches the speed of light, the radiation is beamed increasingly forward and is strongly polarised.

3.4 Properties Affecting Emissions

Many aspects of the neutron star's geometry affect the emissions that will be seen by a distant observer, such as us here on Earth. Table 2 shows some properties of the simulated stars which were investigated.

Property	Possible Values	Values Used
Observer Viewing Angle	$0° - 180°$	$0° - 180°$
Magnetic Inclination Angle, χ	$0° - 180°$	$0° - 90°$
Emission Distance	$0.1 - 0.9R_{LC}$	$0.1 - 0.9R_{LC}$
Polar Cap Band Width	$0° - \theta_{PC}$	$0.2°$
Emissions Spread	$0° - \sim 5°$	Gaussian, $\sigma = 3°$

Table 2: Neutron Star Properties Affecting Emissions

However, it is not even as simple as varying these parameters until we find a plot of emissions which matches observations. We have yet to figure out how field lines (in particular emitting field lines) are distributed over the polar cap. We also do not know the distribution of the scattering of emissions from the field line (Gaussian was assumed for this project). Further we do not know if emission occurs at a spherical distance from the star, as opposed to a fixed distance along field lines, or perhaps a fixed distance to the light cylinder.

4 Design of Program

All the code was written in Python version 2.7 on Ubuntu Linux. Python was chosen as it is an easy language to learn and use allowing the code written to be easily adapted and updated in future projects. Packages used were:

- **Numpy** The Numpy package was used to manage the arrays storing the emissions information as it has many features specially designed for working with large amounts of data.
- **SciPy** The Gaussian filter from scipy.ndimage.filters was used to model the spread of emissions from each field line as this works directly with Numpy arrays.
- **VPython** The VPython or Visual Python package was used in creating the 3D visualisations of the star and magnetic field. The 'vector' objects from this package were also used as they create a close resemblance between the code and the equations.
- **MatPlotLib** The mathematics plotting library or MatPlotLib was used to plot the emissions.
- **Tkinter** Used by the above two packages for creating windows with which to display graphs and visualisations.

Instructions for downloading and running the code are included in the appendix.

4.1 Classes

In order to allow the program to be as adaptable as possible and to carry out the distinct principle tasks for this project with most ease, it was necessary to make use of Python's Object Oriented Programming features. Two classes were created, 'Star' and 'Fieldline', allowing for the storing of information about objects of these types in a very logical and organised way.

4.1.1 'Star' class

The 'Star' class, contained in the file *classStar.py*, allows for the creation of Star objects. On creating a star, some features are assumed unless otherwise declared. Features which must be given are radius, period of rotation and magnetic inclination angle. B_0 the magnetic strength at the poles and ξ the dimensionless magnetic colatitude of open field lines are assumed to have values of 1 and 0.9 respectively unless otherwise declared. Also upon creation some properties of the star are calculated from the information given. These include η_{lc} the light cylinder radius normalised by the radius of the star, Ω the stellar angular velocity and κ the parameter measuring general-relativistic effect of frame dragging at the stellar surface in units of stellar angular velocity. This class contains several functions, the primary function being to draw the star. This makes use of the previously declared and calculated properties to draw the 3D visualisation of the star, the light cylinder and the rotation axis.

4.1.2 'Fieldline' class

The 'Fieldline' class is designed in the file *classFieldline.py*. This class allows for the creation of field line objects which represent a single field line (using the Muslimov and Harding Model for the magnetic field [Muslimov and Harding, 2005]). To create a field line three parameters are required: the star from which the field line originates and the azimuthal and polar angles of its initial position. The first optional parameter *emissionRadPercentLC* takes a list of distances (as a percentage of the light cylinder radius R_{LC}) at which to calculate the direction of emissions (default is $0.5R_{LC}$). The other optional parameter *rep*, gives a limit to how many increments of calculating the field line can be made before moving on the next field line. This will only be used in cases where field lines start very close to the pole and are taking too many iterations to return to the star or hit the light cylinder.

When a field line is created, its initial position is calculated from the radius of the star and the values passed for theta and phi. Then the magnetic field direction at this position is calculated, and the position vector is updated to a unit length (1 stellar radius) in this direction. This process repeats until the field line is past the light cylinder, has returned to the star or, if *stopAtEmission* is True, when emission occurs. For this reason, *stopAtEmission* must be set to False if coordinates of the polar cap are unknown as the field line must continue until it encounters the light cylinder or returns to the star.

Field line objects have properties such as *emissionDirections*, which returns a list of emissions directions of the field line for each emission distance, and *isOpen* which returns True if it is an open field line, False otherwise.

```
myStar = Star(10, 0.3, 30) #creating a Star with radius 10km, period 0.3s, χ = 30°
polarCapAngles = [ ]
for phi in range(0, 360):
    theta = 0
    myFieldline = Fieldline(myStar, phi, theta) #Fieldline with initial position (θ, φ)
    while myFieldline.isOpen:
        theta += 0.1
        myFieldline = Fieldline(myStar, phi, theta)
    polarCapAngles += [theta]
print(polarCapAngles)
```

Figure 4: A sample algorithm using the created classes to find the shape of the polar cap

4.2 Algorithms

4.2.1 Calculation of Field Lines

When a 'Fieldline' object is created, the points through which it passes are calculated using the following method:

1. Store current position
2. Calculate magnetic field at initial position
3. Find point one stellar radius in magnetic field direction
4. Repeat until hit the light cylinder, back at the star, or maximum increments have occurred

Initially, the dependence of field strength on radial distance of r^{-3} was used to scale the size of the increments. Though this lead to very small increments at just a small fraction of the light cylinder radius from the star resulting in the program requiring thousands of iterations to form a single closed field line.

4.2.2 Determining Observer's View of Emissions

The emission direction of an individual field line was determined by following the field line until it reached emission distance from the star. At this point the direction of the field line was converted into polar coordinates with polar axis parallel to the rotational axis and then stored as part of the field line object. Any number of emissions directions can be stored in a field line in order of nearest to furthest emission distance.

To determine emissions seen by an observer, field lines were calculated for many initial positions by incrementing through phi and theta angles. The emission directions of these field lines were stored in a 180 x 360 array by incrementing the number at the position corresponding to the direction of emission. A separate array was used for each emission distance. After this was

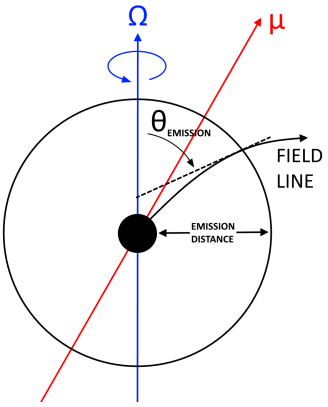

Figure 5: Algorithm for calculating direction of emissions from a field line.

repeated for all initial positions, the final array was output as a picture. With the colour at each point corresponding to the intensity of emissions seen by an observer at a particular angle from the axis of rotation, at a particular point in the star's rotation. The spreading of emissions from each field line is taken into account after calculations using a Gaussian blur on the emissions arrays.

4.2.3 Storing and Retrieving Emissions Results

Emissions are stored in a 180 x 360 array, where the value at each point represents the emissions received in the region. Emissions from a single emission distance can be saved to a single file. This is done without any blurring being applied to the array which allows for changing the scattering of emission from field lines for an already computed array. Functions for systematic naming of files were written to allow organised storage and retrieval of emissions data.

4.3 Optimisations

As all of the simulations for this project were computed on a laptop[2], optimising the program to run as efficiently as possible was a priority. Trigonometric functions for each of the angles χ, ϕ, θ were calculated and stored as variables at the start of each loop as these were used approximately 80 times in the equations to calculate the magnetic field at a point. Further, the equations greatly simplify for the case of the aligned rotator ($\chi = 0\,\text{deg}$), so the simplified equations for this case were written into the code separately allowing much faster calculations for this particular case.

Each of the properties affecting emissions which were cycled through were taken into account using different methods, many of which lend themselves to optimisation. A single field line only has to be calculated once to determine its direction of emissions at any distance from the star. This allows emissions from several emissions distances for a particular star to be calculated at the same time. Scattering of emissions from field lines is not applied to stored emissions. This means that each time saved emissions are retrieved from a file, a different distribution and magnitude of emissions scattering can be used. Practically no computation time is required to do this, provided the saved emissions file exists.

[2]Processor: Intel(R) Core(TM) i7-4510U CPU @ 2.60 GHz, RAM: 8.00 GB

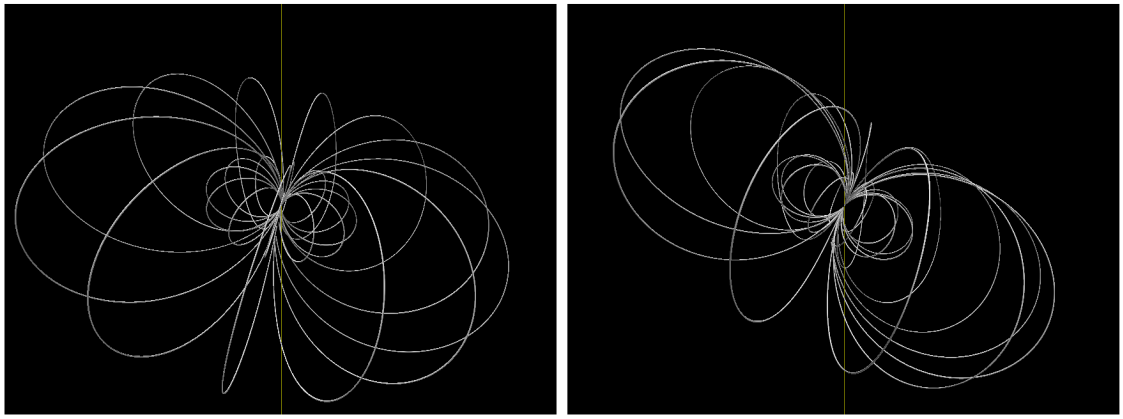

Figure 6: 3D visualisation of magnetic field using VPython package.

A method was discovered which allowed computation of emissions for multiple stars at once. It was possible to run computations in parallel by running several versions of the program simultaneously, each one calculating emissions for a star with a different magnetic inclination angle. The computer would then use its built in process manager to allocate these computations to the various cores. It is advised for future work that multi-threading be written into the code to allow for more optimised and adaptable computing.

5 Results

5.1 Visualisation

The vpython package gave excellent results for the 3D animation of the star. The user can zoom in/out, rotate the star on the screen allowing for viewing of the magnetic field from any angle or even have the star animated to spin around its rotation axis. Combined with the designed code, which allows for specifying the parameters of the star, this gives a practical and accurate representation of any star.

5.2 Polar Cap Shape

The polar cap shape for a neutron star with period 0.033 s was investigated for different magnetic inclination angles using an optimised version of the algorithm seen in Figure 4. This showed the polar cap to be elliptical in shape for small magnetic inclination angles, becoming elongated in the direction of rotation of the star as this angle increased until 90° where it is egg shaped with the wider area towards the direction of rotation. For small magnetic inclination angles it was seen that several polar cap points at $\phi \approx 115°, 285°$ were not aligned with the rest, instead being slightly further towards the magnetic axis. This could be due to the way that the computer calculates trigonometric functions, and it was suggested that an interpolation approach could be used if this is the case. Another notable feature of the polar cap shape is the dip in the polar cap circumference which can been seen on the southern edge of the cap for most magnetic inclination angles.

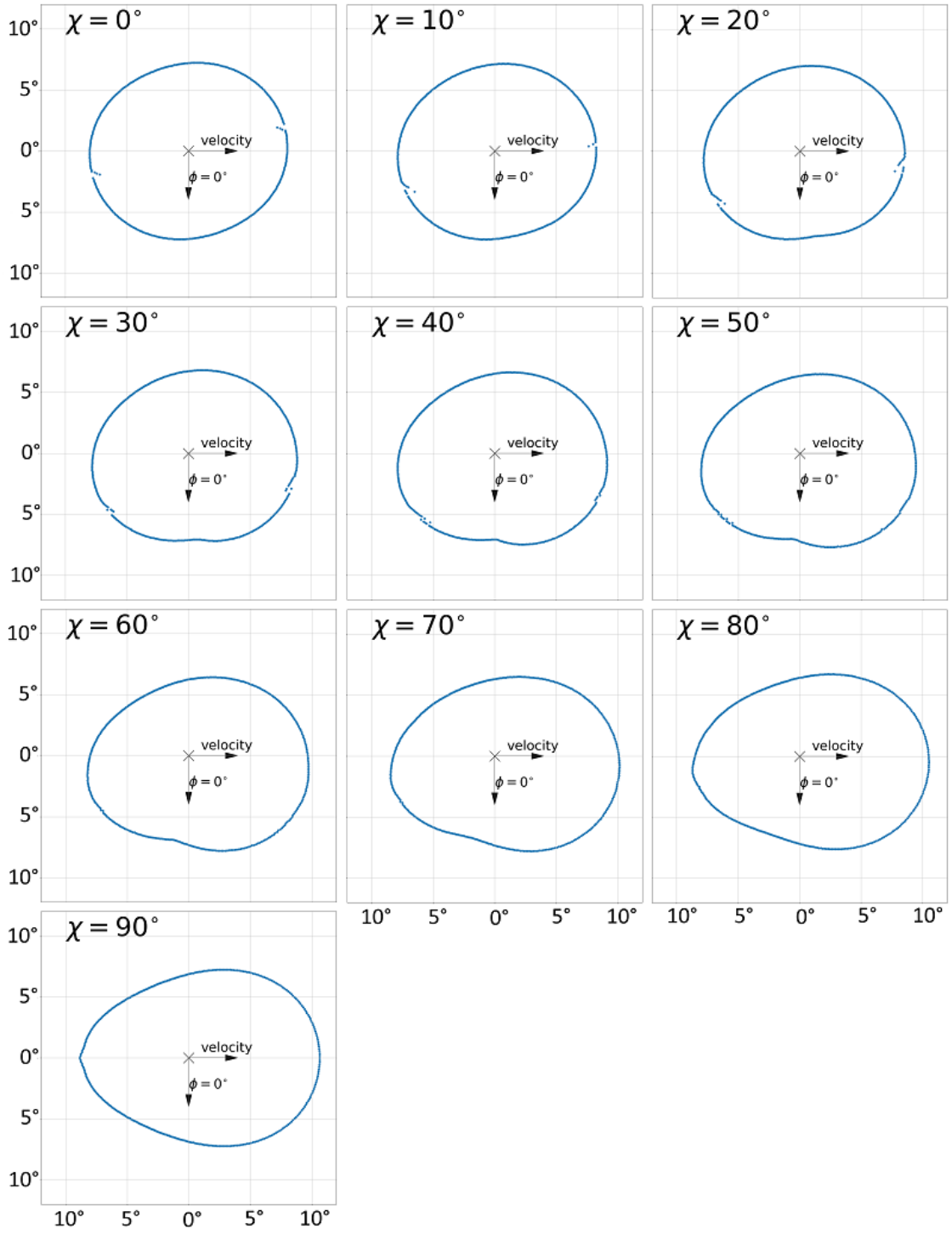

Figure 7: Polar cap shape for varying magnetic inclination angle, rotation period 0.033 s. The magnetic axis is represented by the cross in the centre and the side of each grid square represents a 5° increase in polar angle θ.

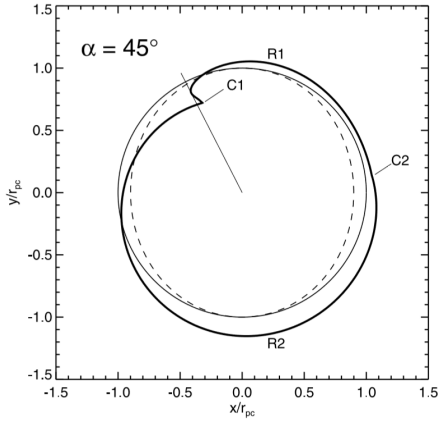

Figure 8: Figure 1 from [Dyks et al., 2004]. Polar cap shape for a dipole tilted at 45° and rotation period 0.033 s. It is rotated at 90° to Figure 7 images; the azimuthal angle is measured counter-clockwise from the positive x-axis and the rotational velocity is directed upward. "The thick solid line (with a notch) presents the polar cap rim for the retarded dipole. The dashed oval is for the static shape dipole. A circle of radius r_{pc} (corresponding to a polar cap of a dipole aligned with rotation axis) is added for a reference (thin solid line)."

A 2004 paper [Dyks et al., 2004] shows similar results for the shape of the polar cap for a neutron star with period 0.033 s and magnetic inclination angle of 45° (see Figure 8). In this paper a bisection method was used, with a small modification from previous attempts to avoid discontinuities. The dip in the edge of the polar cap C2 can been seen at $\phi = 0°$, as well as the egg shaped bulging. This paper highlights the 'notch' C2 with particular interest. It is noted that the polar cap appears to be made up of two different curves which meet at points C1 and C2. It is possible that the unaligned points seen in the results of this project for small inclination angles are a result of the presence of this notch, but more investigation is required. As the algorithm used stopped upon finding a closed field line, a suitable approach may be to plot many field lines in the areas of interest and noting which are open/closed.

5.3 Emissions Calculations

5.3.1 Plotting Emissions

Emissions from the star were plotted with observers angle to the rotational axis of the star on the y-axis and the azimuthal angle ϕ around the star on the x-axis with the brightness of each point indicating the relative intensity of emissions seen. This allowed clear qualitative investigation of how observed emissions varied with different properties of the star. These graphs can be read by first choosing the observer's viewing angle on the y-axis. The emissions observed over the course of one rotation of the star can then be read from the brightness of the points along a horizontal line from this point. Such plots make it very clear which observers see no emissions, which see emissions with a single peak, and which see emissions with two peaks. It is important to note that these plots represent one rotation of the star, and so are imagined to repeat infinitely in the horizontal direction.

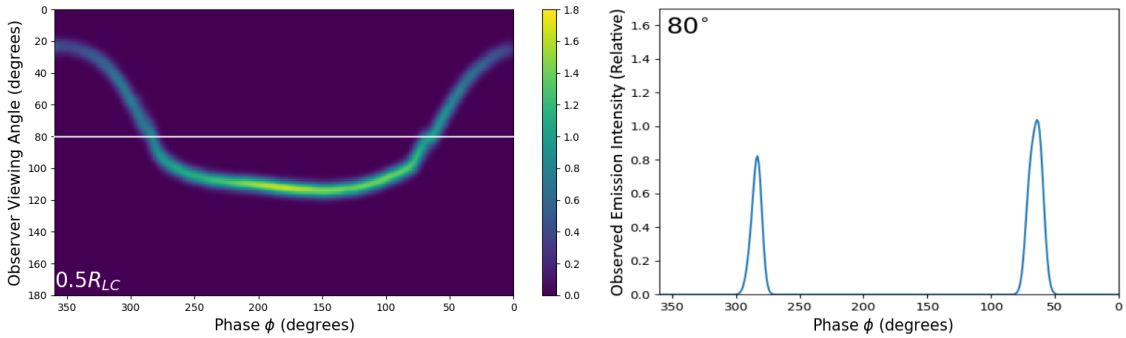

Figure 9: Plot of observed emissions for all viewing angles with corresponding pulse profile for viewing angle of 80°. Magnetic inclination angle $\chi = 45°$, emission distance $= 0.5R_{LC}$.

It is expected that plotting of emissions from the south pole of the star would result in a plots which have similar shape to those from the north pole. These south pole emissions would be flipped through the x-axis and shifted by a phase of 180° relative to the north pole emissions.

5.3.2 Varying Magnetic Inclination Angle, χ

Emissions plots were created for stars with magnetic inclination angles between 0° and 90° in steps of 10°. Emission distance was held fixed at $0.5R_{LC}$, with a polar cap band width of 0.2° for a star with period 0.033 s. From these plots (Figure 10) it can be seen that as magnetic inclination angle is increased, more angles of observation will see pulses. It is also noticed that observers at a viewing angle close to 90° would not see a change in the time between pulses for different magnetic inclination angles, with distance between pulses changing dramatically (generally to more equally space the pulses) for observers with much smaller viewing angles.

At $\chi = 90°$, the shape of emissions is very similar to the polar cap shape for this magnetic inclination. This is expected due to the symmetry of the effect of rotation on the field lines when the magnetic axis is perpendicular to the rotation axis.

Another interesting feature of these plots which can be seen as a product of the polar cap shape is the notches which appear at small magnetic inclination angles. These form at $\phi \approx 90°, 270°$ and seem to correspond with the notches seen in the rim of the polar cap for small inclination angles. As noted in the polar cap results, this effect could be due to a physical phenomenon or a computational effect.

5.3.3 Varying Emission Distance, R_{LC}

Variation in observed emissions with emission distance was also investigated. Emission distance was incremented from $0.1R_{LC}$ to $0.9R_{LC}$ in steps of $0.1R_{LC}$. Magnetic inclination angle was fixed at $\chi = 45°$ and polar cap band width at 0.2° for a star with period 0.033 s. It was seen (Figure 11) that between $0.3R_{LC}$ and $0.9R_{LC}$, the emissions plot roughly held its shape but moved towards increased observer viewing angles. This would result in an observer viewing a change in pulse width of the pulses coming closer together as emission distance in increased. For an emission

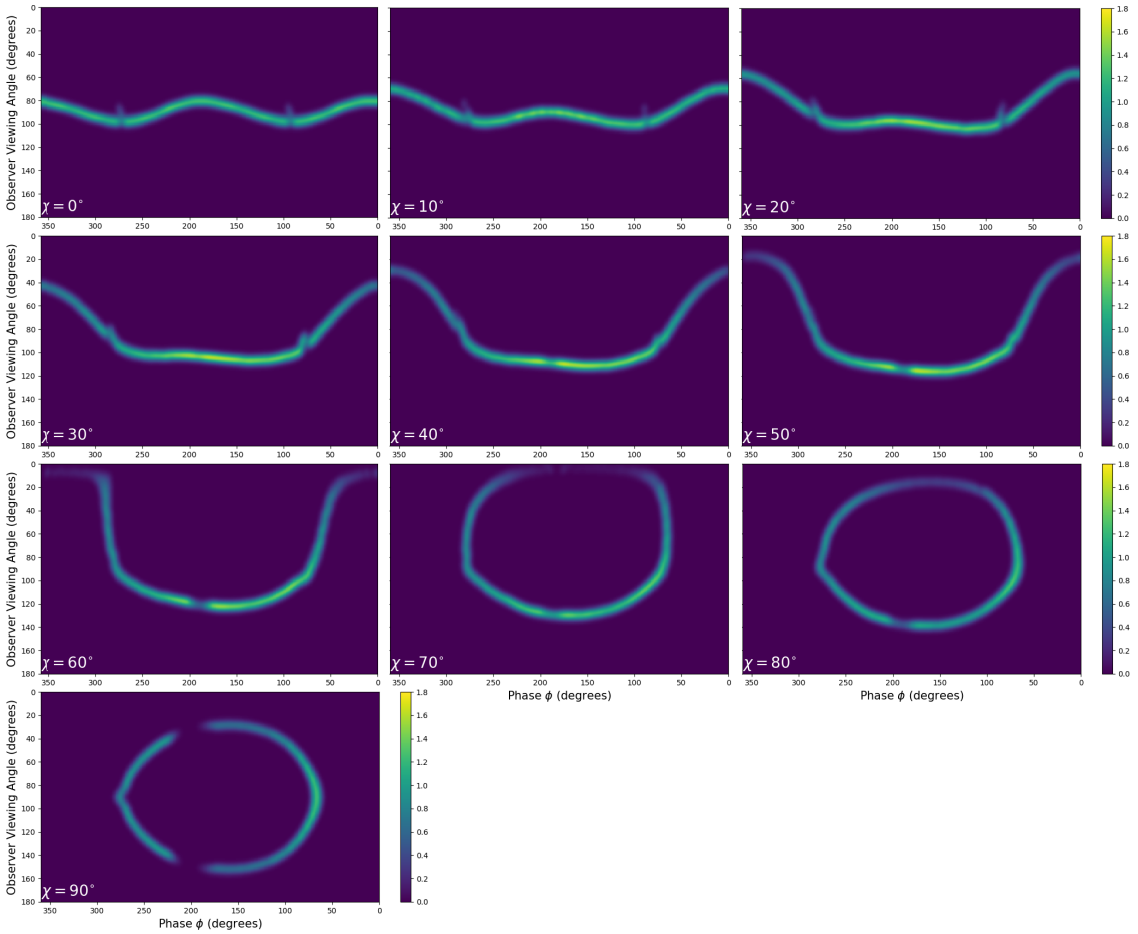

Figure 10: Effect of varying magnetic inclination angle χ. Emission distance fixed at $0.5R_{LC}$.

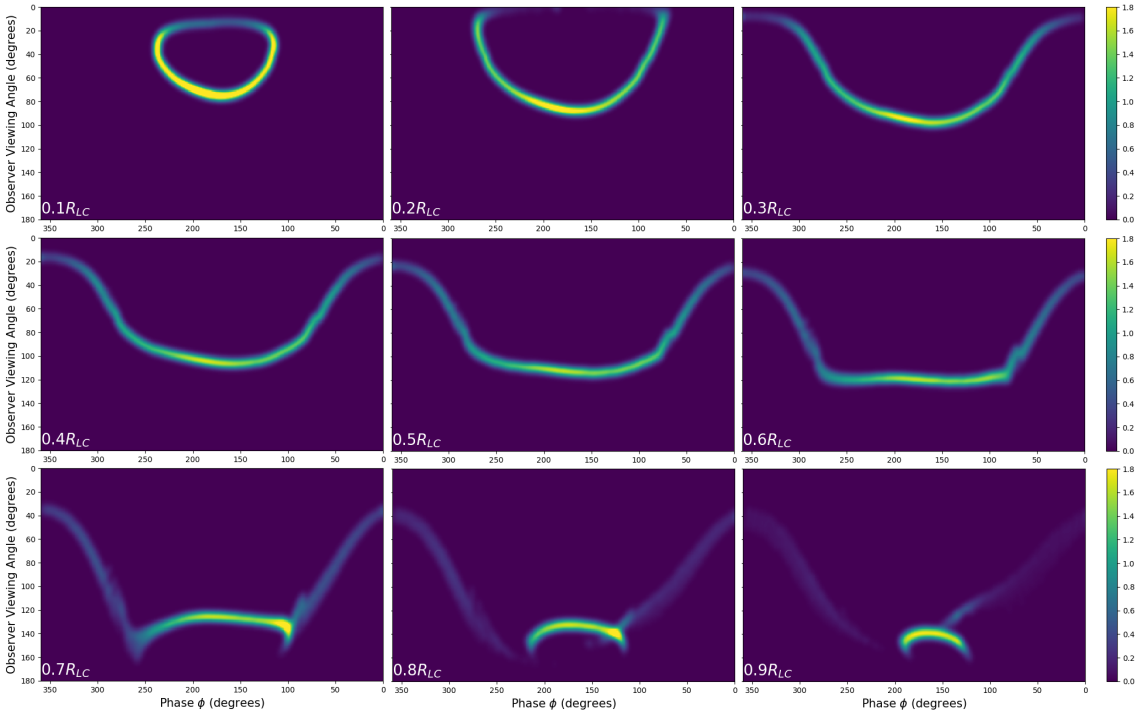

Figure 11: Effect of varying emission distance from $0.1R_{LC} - 0.9R_{LC}$. Magnetic inclination angle fixed at $\chi = 45°$.

distance less than $0.3R_{LC}$, many observer angles do not view any emissions. As emission distance is decreased from this point, pulses become very distinct, bright and close together.

5.4 Comparison to Observed Emissions: Crab Pulsar

The magnetic inclination angle and viewing angle are not known for certain for any observed neutron star, so this model was compared to actual observations using the best estimates of inclination and viewing angle for the Crab Pulsar. A 2004 paper estimates the magnetic inclination to be $\sim 61°$ [Ng and Romani, 2004], while a 2008 paper estimates the magnetic inclination of the crab to be $\sim 45°$ with a viewing angle of either $80°$ or $100°$ [Harding et al., 2008]. Using the program described earlier, emissions were calculated for each of these cases and compared to actual observations of the Crab pulsar taken by the FERMI Large Area Telescope [Abdo et al., 2009].

As seen in Figure 12, each of these estimates gives approximate but not perfect recreations of the Crab pulse profile using the program from this project. The phase difference of the pulses of $40°$ appears to be matched. The relative heights of the pulses is correct in order, though incorrect in magnitude. Further, the shape of the modelled pulses are quite similar, while the observations show the small pulse to be wider and the taller pulse to be narrower. These predictions might easily be changed by varying the polar cap band width, or the scattering from each field line which were not investigated in this project.

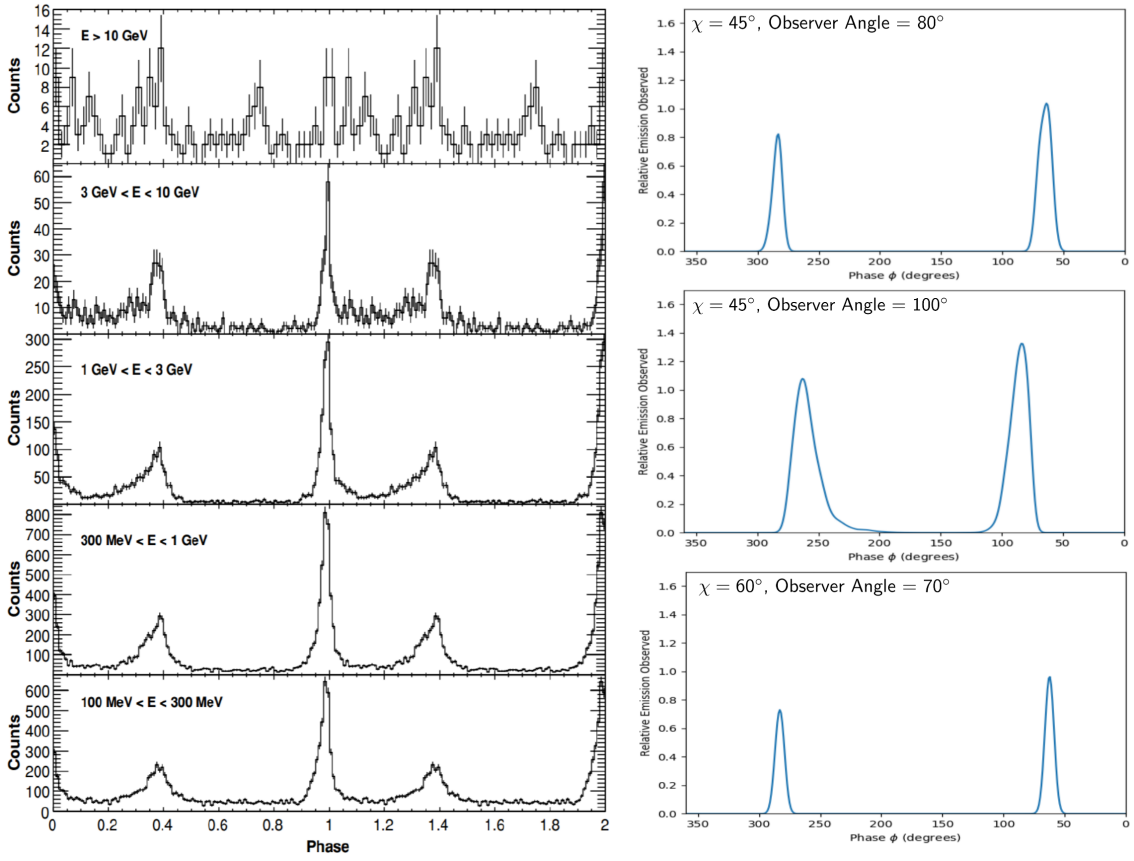

Figure 12: Comparison of observed Crab Pulsar emissions at different energy levels (made by FERMI Large Area Telescope [Abdo et al., 2009]) to pulse profiles predicted with the program from this project using best current estimates for crab magnetic inclination and viewing angles [Ng and Romani, 2004, Harding et al., 2008].

6 Discussion

6.1 Difficulties

The Deutsch model for the magnetic field was not simulated in this project. A comparison between this and the Muslimov and Harding model could have led to identifying important differences which might influence for what research it would be necessary to choose one over the other. The Muslimov and Harding model used magnetic coordinates, whereas Deutsch used coordinates based on the rotational axis. This difference means that a large amount of the current computer program code could not be easily adapted to deal with the Deutsch field and separate code would have to be written.

It is believed that modelling emissions of the star from a length of field line within a region - rather than at an exact distance from the star - will require a considerable amount of additional work. Currently, the star is treated as remaining stationary with the observer rotating about the star's rotational axis. This method does not lend itself to calculating emissions from a region with depth, as the time difference between emissions from across the emission region of an individual field line leads to emissions not arriving to the observer at the same time. This would need to be accounted for by using the rotational velocity of the star to calculate the difference is apparent position of these emissions.

For the duration of this project, a value for the polar cap band of 0.2° was used. The reason that larger band widths were not investigated was due to the clumping of magnetic field lines around the magnetic pole. In the algorithms for calculating emissions, the initial positions of field lines are created by cycling through polar coordinates in equal steps. Due to the nature of polar coordinates, the density of points increases as the polar angle becomes smaller. This means that field lines are created more closely together the closer to the magnetic pole they are. This has the effect of increasing emissions in particular directions. A new coordinate system was devised in order to tackle this problem. This system uses two polar angles; one measured towards the positive x-axis, and the other measured towards the positive y-axis. Incrementing in steps through these angles gives evenly spaced points surrounding the pole. However, this coordinate system is not as intuitive to work with as polar coordinates and not as easy to restrict to a polar cap band. This lead to polar coordinates being used.

6.2 Sources of Error

Initially, the step sizes in the calculation of the magnetic field were proportional to the magnetic field strength. However, this r^{-3} dependence led to extremely large step sizes near the stellar surface, and extremely small step sizes at just a small distance away. Due to the decreasing size of the increments, it would take thousands of iterations for a single field line to return to the star. This approach was too computationally demanding, and so increments were instead decided to be of a unit length = 1 stellar radius. This has consequences for all parts of this project but it is unknown whether or not these are significant. Magnetic field lines are, by definition, the path that a charged particle with no mass would follow when placed in that magnetic field. Perhaps an approach taking into account momentum of the particles is necessary. In this case the r^{-3}

dependence would unlikely have such a dramatic effect on the step size.

κ (represented in the code by the letter k) is the parameter measuring the general-relativistic effect of frame dragging at the stellar surface. This was estimated by Muslimov and Harding [Muslimov and Harding, 2005] using as $\kappa \approx 0.15 I_{45}/R_6^3$ where $I_{45} = I/10^{45} gcm^2, R_6 = R/10^6$ cm, I is the moment of inertia of NS of radius R. However, most modern computers can only do arithmetic with numbers less than 10^{16} decimal places in difference, so this expression was simplified down by hand, using the formulae for the moment of inertia of a solid sphere and a neutron star density of $10^{17} kg/m^3$ to get

$$\kappa = \frac{1}{125}\pi R^2 \tag{5}$$

Later in their paper Muslimov and Harding estimate that $(2\kappa(1-\kappa))^2 \approx 30^\circ$. This would imply that κ has a value of either 0.836 or 0.164. However, the calculations above indicate a value of ~ 2.5. In the code the value of κ is assumed to be 0.836, but function *setOtherk()* included in *classStar.py* will calculate κ using equation (5) above and recalculate any parameters of the star which depend on κ.

6.3 Future improvements

Some additional physical features of emissions which were not modelled in this project are:

- emission from the south pole of the star
- emission from field lines in backwards direction
- emission from a longer section of field line
- polarisation of emissions
- different energy emissions

In the case of south pole and backward direction emissions, these can be easily implemented into the current computer program. In fact, a lot of the code was written with the goal of modelling emissions from both poles. The difficulties of modelling emission from a longer section of field lines are discussed in difficulties section 6.1 above. Modelling of the polarisation or separating emissions of different energies were not looked into during this project. These are all observable features of neutron stars and therefore would lead to testable results.

On the computational side, several major improvements could be made. The first of these would be making use of the new coordinate system discussed in the difficulties section 6.1 to create a more even distribution of field lines over the polar cap. Introducing more optimisations such as multi-threading or calculating for several polar cap band widths at once. The latter could be done by storing the corresponding field line initial position for each emission direction. Then, after the calculations have run, different restrictions could be put on the initial positions of emitting field lines and the resulting emission directions calculated instantly, without having to run the entire program again. The ideal scenario would be to have every field line starting point and the corresponding emission direction of each already calculated for various emission distances and magnetic

inclination angles. This would allow a database of results to be queried and emissions plots formed immediately without having to run entire simulations.

Another possibility for improvement could be to implement statistical tests to compare the calculated emissions with observations in order to determine correctness of the magnetic field and emission models and determine our viewing angle to real pulsars.

A similar program could be written to model the shape and the emissions seen using a Deutsch field. A comparison of those results and the results of this project using the model designed by Muslimov and Harding could be very useful in helping researchers determine whether changing the magnetic field model they use will have an effect on their research.

7 Conclusion

The aims of this project were achieved and surpassed. Clear visualisations of the neutron star magnetic field were created and the changing of polar cap shape, emissions observed for stars with different properties and how these emissions change as particular properties of the star are varied were studied with clear visualisations being made for these also. Further, the computer program designed during this project allows for various other investigations to be carried out using a straightforward system. All results which could be compared to observations and previous publications appear to be in agreement with these. The tools and results of this project will contribute to research at NUI Galway, and can be developed further in the future as our knowledge of neutron stars develops.

Appendix

Muslimov and Harding Equations

Magnetic field is based on a pure dipole with corrections added:

$$\mathbf{B} = \mathbf{B}^d + \mathbf{B}^{(1)} + \mathbf{B}^{(2)} + \mathbf{B}^{(2*)}$$

Basic pure dipole geometry:

$$\mathbf{B}^{\rm d} = \frac{B_0^{\rm d}}{\eta^3}\ \left(\ \cos\theta\ \mathbf{e}_{\rm r} + \frac{1}{2}\ \sin\theta\ \mathbf{e}_\theta\ \right)$$

First-order correction for charge flow along the open field lines, $\mathbf{B}^{(1)}$:

$$B_r^{(1)} = \frac{3}{2}\left(\frac{\eta}{\eta_{\rm lc}}\right)\ \frac{B_0^{\rm d}}{\eta^3}\ \theta_0\ \xi\ (1-\theta\cot\theta)\sin\chi\sin\phi,$$

$$B_\theta^{(1)} = -\frac{3}{2}\left(\frac{\eta}{\eta_{\rm lc}}\right)\ \frac{B_0^{\rm d}}{\eta^3}\ \theta_0\ \xi\ \left(\frac{\theta-\sin\theta\cos\theta}{\sin^2\theta}\right)\sin\chi\sin\phi,$$

$$B_\phi^{(1)} = -\left(\frac{\eta}{\eta_{\rm lc}}\right)\ \frac{B_0^{\rm d}}{\eta^3}\ \left[(1-\kappa)\cos\chi\sin\theta + \frac{3}{2}\theta_0\xi\left(\frac{\sin^3\theta+\sin\theta-\theta\ \cos\theta}{\sin^2\theta}\right)\sin\chi\cos\phi\right]$$

Second-order correction due to distortion caused by rotation of dipole field, $\mathbf{B}^{(2)}$:

$$\begin{aligned} B_{\rm r}^{(2)} &= \left(\frac{\eta}{\eta_{\rm lc}}\right)^2\ \frac{B_0^{\rm d}}{\eta^3}\ \cos\theta\ \Big\{\cos\chi\ [\cos\chi\ \sin^2\theta + 2\ \Lambda_0\ (1-\kappa)] + \sin^2\chi\ \left(1-\frac{1}{2}\ \sin^2\theta\right) - \\ &\quad 2\ \left[\cos\chi\ \sin\theta\ \cos\theta + \frac{3}{2}\ \Lambda_0\ \theta_0\ \xi\ \left(\frac{\theta}{\sin\theta\ \cos\theta} - 1\right)\right]\ \sin\chi\ \cos\phi - \\ &\quad \frac{1}{2}\ \sin^2\chi\ \sin^2\theta\ \cos 2\phi\Big\}, \end{aligned}$$

$$\begin{aligned} B_\theta^{(2)} &= -\left(\frac{\eta}{\eta_{\rm lc}}\right)^2\ \frac{B_0^{\rm d}}{\eta^3}\ \sin\theta\left\{\left[\frac{1}{4}\cos\chi\ \sin^2\theta + \Lambda_0\ (1-\kappa)\right]\ \cos\chi + \right. \\ &\quad \frac{1}{2}\ \sin^2\chi\ \left(1-\frac{1}{4}\ \sin^2\theta\right) + \left[\left(\frac{1}{4}\ \cot\theta\ \cos 2\theta + \frac{1-\cos\theta}{\sin^3\theta}\right)\ \cos\chi - \right. \\ &\quad \left.\frac{3}{2}\ \Lambda_0\ \theta_0\ \xi\ \left(\frac{3(1-\theta\ \cot\theta)}{\sin^2\theta} - 1\right)\right]\ \sin\chi\ \cos\phi - \\ &\quad \left.\frac{5}{8}\left[\frac{1}{\sin^2\theta}\left(\frac{1-\cos\theta}{\sin^2\theta} - \frac{1}{2}\right) + \frac{1}{5}\sin^2\theta\right]\ \sin^2\chi\ \cos 2\phi\ \right\}, \end{aligned}$$

$$\begin{aligned} B_\phi^{(2)} &= \left(\frac{\eta}{\eta_{\rm lc}}\right)^2\ \frac{B_0^{\rm d}}{\eta^3}\ \left\{\left[\left(\frac{1}{4}+\frac{1-\cos\theta}{\sin^2\theta}\right)\ \cos\chi + \frac{3}{2}\ \Lambda_0\ \theta_0\ \xi\ \frac{3\ \sin\theta\ \cos\theta - \theta\ (3-2\ \sin^2\theta)}{\sin^2\theta}\right]\times\right. \\ &\quad \left.\sin\chi\ \sin\phi - \frac{5}{8}\ \left(\frac{1-\cos\theta}{\sin^3\theta} - \frac{1}{2\ \sin\theta}\right)\ \sin^2\chi\ \sin 2\phi\right\}, \end{aligned}$$

Second-order correction due to distortion generated by $\mathbf{E} \times \mathbf{B}$ drift of out-flowing charges, $\mathbf{B}^{(2*)}$:

$$B_{\rm r}^{(2*)} = -2 \left(\frac{\eta}{\eta_{\rm lc}}\right)^2 \frac{B_0^{\rm d}}{\eta^3} \Lambda_0 \ (\cos\chi \ \cos\theta + \sin\chi \ \sin\theta \ \cos\phi)$$

$$B_{\theta}^{(2*)} = \left(\frac{\eta}{\eta_{\rm lc}}\right)^2 \frac{B_0^{\rm d}}{\eta^3} \Lambda_0 \ (\cos\chi \ \sin\theta - \sin\chi \ \cos\theta \ \cos\phi)$$

$$B_{\phi}^{(2*)} = \left(\frac{\eta}{\eta_{\rm lc}}\right)^2 \frac{B_0^{\rm d}}{\eta^3} \Lambda_0 \ \sin\chi \ \sin\phi.$$

Here, $\Lambda_0 = (1-\kappa)\cos\chi + (3/2)\theta_0\xi\sin\chi\cos\phi_{pc}^0$ which comes from the current density in the electrodynamic model of [Muslimov and Tsygan, 1992]. κ measures the general-relativistic effect of frame dragging at the stellar surface and is calculated as discussed in section 6.2. ξ is the dimensionless magnetic colatitude of open field lines and ranges from $\xi = 0$ at the magnetic axis to $\xi = 1$ for the last open field lines. $\theta_0 \approx (\Omega R/c)^{1/2}$ is the canonical polar cap half-angle. $\theta, \phi, \chi and \eta$ are as discussed in section 2.3.1.

Downloading and running the program

To use the code written during this project, you will first need to install Python2.7 [3]. The code can be downloaded from the GitHub repository [4]. The following python packages will also need to be installed:

- Visual Python - `http://vpython.org/`
- Tkinter
- Matplotlib

The easiest way to do this is using pip, the python package manager, which installs as part of Python2.7. Use the following pip commands in command prompt or terminal:

- pip install vpython
- pip install tk
- pip install matplotlib

Once these are installed, open the file *main.py* in the project code using a text editor and copy/paste an already written function into the main statement (clearer instructions are provided in the code, and on the GitHub page for this). Alternatively, a new function can be created here using the designed classes/functions. The program can then be run by navigating to the downloaded directory in terminal or command prompt and running the command:

- python main.py

[3] `https://www.python.org/downloads/release/python-2713/`
[4] `https://github.com/jackmpcollins/Neutron-Star-Magnetosphere`

Bibliography

References

[Abdo et al., 2009] Abdo, A., Ackermann, M., Ajello, M., Atwood, W., Axelsson, M., Baldini, L., Ballet, J., Barbiellini, G., Baring, M., Bastieri, D., et al. (2009). Fermi large area telescope observations of the crab pulsar and nebula. *The Astrophysical Journal*, 708(2):1254.

[Babcock and Cowling, 1953] Babcock, H. and Cowling, T. (1953). General magnetic fields in the sun and stars (report on progress of astronomy). *Monthly Notices of the Royal Astronomical Society*, 113:357–381.

[Becker et al., 2009] Becker, W. et al. (2009). Neutron stars and pulsars.

[Cheng et al., 1986] Cheng, K., Ho, C., and Ruderman, M. (1986). Energetic radiation from rapidly spinning pulsars. i-outer magnetosphere gaps. ii-vela and crab. *The Astrophysical Journal*, 300:500–539.

[Cowling, 1952] Cowling, T. (1952). The oscillation theory of magnetic variable stars. *Monthly Notices of the Royal Astronomical Society*, 112(5):527–539.

[de Burca, 2016] de Burca, D. (2016). *Polarisation of synchrotron radiation from isolated neutron stars*. PhD thesis, National University of Ireland, Galway.

[Deutsch, 1955] Deutsch, A. J. (1955). The electromagnetic field of an idealized star in rigid rotation in vacuo. In *Annales d'Astrophysique*, volume 18, page 1.

[Dyks et al., 2004] Dyks, J., Harding, A. K., and Rudak, B. (2004). Relativistic effects and polarization in three high-energy pulsar models. *The Astrophysical Journal*, 606(2):1125.

[Gold, 1968] Gold, T. (1968). Rotating neutron stars as the origin of the pulsating radio sources. *Nature*, 218:731–732.

[Goldreich and Julian, 1969] Goldreich, P. and Julian, W. H. (1969). Pulsar electrodynamics. *The Astrophysical Journal*, 157:869.

[Harding et al., 2008] Harding, A. K., Stern, J. V., Dyks, J., and Frackowiak, M. (2008). High-altitude emission from pulsar slot gaps: the crab pulsar. *The Astrophysical Journal*, 680(2):1378.

[Hessels et al., 2006] Hessels, J. W. T., Ransom, S. M., Stairs, I. H., Freire, P. C. C., Kaspi, V. M., and Camilo, F. (2006). A Radio Pulsar Spinning at 716 Hz. *Science*, 311:1901–1904.

[Landau, 1938] Landau, L. D. (1938). Origin of stellar energy. *Nature*, 141:333.

[Lorimer and Kramer, 2005] Lorimer, D. R. and Kramer, M. (2005). *Handbook of pulsar astronomy*, volume 4. Cambridge University Press.

[Moran, 2014] Moran, P. (2014). *Multi-wavelength and Polarisation Studies of Pulsars: the Crab, Vela, and PSR J0205+6449*. PhD thesis, National University of Ireland, Galway.

[Muslimov and Tsygan, 1992] Muslimov, A. and Tsygan, A. (1992). General relativistic electric potential drops above pulsar polar caps. *Monthly Notices of the Royal Astronomical Society*, 255(1):61–70.

[Muslimov and Harding, 2005] Muslimov, A. G. and Harding, A. K. (2005). Effects of rotation and relativistic charge flow on pulsar magnetospheric structure. *The Astrophysical Journal*, 630(1):454.

[Ng and Romani, 2004] Ng, C.-Y. and Romani, R. W. (2004). Fitting pulsar wind tori. *The Astrophysical Journal*, 601(1):479.

[O'Connor, 2004] O'Connor, P. (2004). *An 'inverse mapping' approach to nonthermal optical emission from isolated spin-powered neutron stars*. PhD thesis, National University of Ireland, Galway.

[Romani and Yadigaroglu, 1994] Romani, R. W. and Yadigaroglu, I.-A. (1994). Gamma-ray pulsars: Emission zones and viewing geometries. *arXiv preprint astro-ph/9401045*.

[Shapiro and Teukolsky, 2008] Shapiro, S. L. and Teukolsky, S. A. (2008). *Black holes, white dwarfs and neutron stars: the physics of compact objects*. John Wiley & Sons.

[Wiedemann, 2003] Wiedemann, H. (2003). Synchrotron radiation. In *Particle Accelerator Physics*, pages 300–336. Springer.

[Yakovlev et al., 2013] Yakovlev, D. G., Haensel, P., Baym, G., and Pethick, C. (2013). Lev landau and the concept of neutron stars. *Physics-Uspekhi*, 56(3):289.